FINITE ELEMENT FAILURE ANALYSIS OF AN INTERNAL COMBUSTION GAS ENGINE INSERT

Luís Felipe Guimarães de Souza
Pedro Manuel Calas Lopes Pacheco
CEFET/RJ - Department of Mechanical Engineering
20.271.110 - Rio de Janeiro - RJ - Brazil
E-Mail: lfelipe@cefet-rj.br, calas@cefet-rj.br

Abstract. *Internal combustion engine components experiment severe thermomechanical loading cycles. This complex loading history can promote the nucleation and propagation of cracks in mechanical components. Residual stress has an important role in the structural integrity of a mechanical component subjected to such loading. In this work, numeric simulations with a thermoelastic finite element model are used to estimate the residual stress distributions that are present in a stainless steel gas engine insert after the assembly process. This component is assembled in the prechamber engine cylinder head with interference through a process involving subzero cooling, which promotes the development of residual stresses. The numerical results indicate that the presence of residual stresses promoted by the assembly process modify significantly the stress distribution in the component during operation and contributes to the nucleation and propagation of cracks in some critical areas. Metallographic and surface fracture analyses of an insert that failed after 6000 hours of operation shown the presence of cracks in these critical regions. In association to residual stress and such critical regions, it was observed the presence of martensite formed due to the subzero cooling applied for interference assembly technique. The martensitic structure can be developed from retained austenite normally present in this type of steel without a stabilization heat treatment. The low toughness of martensite in association to residual stress in the critical regions has contributed to the failure of the component.*

Keywords: *Failure Analysis, Finite Element, Modeling, Thermomechanical coupling.*

1. Introduction

Internal combustion engine components are in general submitted to a severe and complex thermomechanical loading history. This loading condition requires a careful analysis of the component comprising various areas of knowledge. For the materials standpoint, phenomena associated with phase transformation, corrosion and fatigue must be considered (ASM, 1975). For the structural integrity standpoint, complex effects as the coupling between thermal and mechanical phenomena, know as thermomechanical coupling, must be considered. Large temperature gradients and non-uniform cooling/heating can promote high levels of stresses in the components. The prediction of such stresses distributions is a rather difficult task (Boley and Weiner, 1985; Pacheco, 2001 *et al.*). Also, it is well know that residual stress plays a preponderant part in the structural integrity of a mechanical component, especially in nucleation and propagation of cracks (Fuchs and Stephens, 1980; SAE, 1988; Almer et al., 2000; Webster and Ezeilo, 2001; Pacheco et al., 2001, 2002). Tensile residual stresses can be especially dangerous since fatigue cracks usually propagate by tensile stress field. In the presence of tensile stresses promoted by the normal loading conditions, both stresses are added resulting in much higher tensile stress levels than the ones predicted by the design process. On the other way, compressive residual stresses can be beneficial if, during operation, it is subtracted from tensile stresses generated by the operational loading. Therefore, a detailed knowledge of the residual stress field is required for an accurate assessment of a mechanical component integrity. However, traditional design methodologies of mechanical components do not consider such effects and simplified models are used with high safety coefficients.

This work presents a failure analysis of an internal combustion martensitic stainless steel gas engine insert. This component is assembled in the prechamber engine cylinder head with interference through a process involving subzero cooling. The component is made of SAE 51410 martensitic stainless steel and is shown in Fig. (1). Figure (2) shows the geometry and dimensions of the component. Several engines failed after about 6000 hours of operation. During the engine disassembly, it was found the presence of through-thickness cracks in the prechamber insert. It is believed that these through-thickness cracks allowed the leakage of engine cooling fluid to the engine prechamber resulting in the premature failure of the equipment. The failure analysis started with a material characterization, involving chemical, hardness and metallographic analysis followed by surface fracture analyses. Finally, numeric simulations with a thermoelastic finite element model were used to estimate the residual stress distributions present in a stainless steel gas engine insert after the assembly process with interference and the stress distribution during operation.

Figure 1. Internal combustion stainless steel gas engine insert.

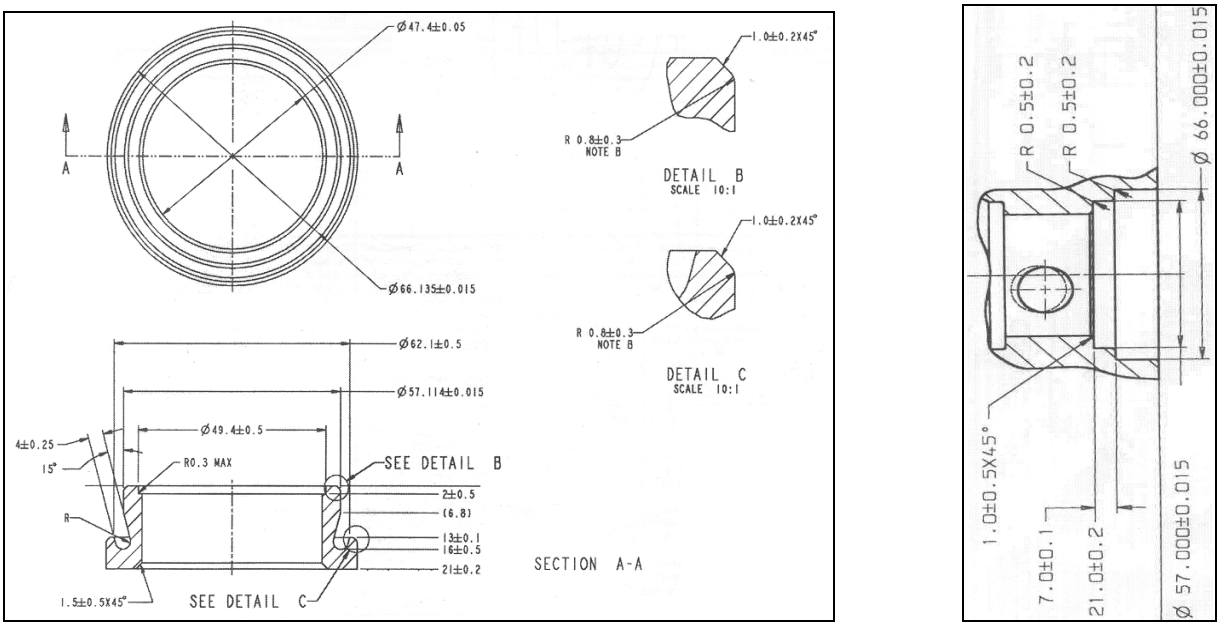

(a) (b)

Figure 2. Internal combustion stainless steel gas engine insert geometry and dimensions. Insert (a) and prechamber engine cylinder (b).

2. Material Characterization

Two inserts, named insert 1 and insert 2, which failed in service, were examined for material characterization by chemical analysis, hardness test and metallographic examination.

2.1. Chemical Analysis

Table (1) shows the results of chemical analysis of the two inserts and compares its result to SAE 51410 specification (Unterweiser et al, 1982). It can be observed that the inserts are in accordance to SAE 51410 specification as proposed for the component.

Table 1 – Chemical Analysis by Optical Emission Spectrometry

Material		Element (weight, %)					
		C	Mn	Si	P	S	Cr
Insert 1		0.138	0.42	0.382	0.017	0.004	11.93
Insert 2		0.133	0.42	0.382	0.017	0.004	11.90
SAE 51410	Min.	-	-	-	-	-	11.5
	Max.	0.15	1.00	1.00	0.040	0.030	13.50

2.2. Metallography

Figure (3) shows the general appearance in the as received condition of the samples that failed in service. Insert 1 was cleaned by shot penning, and insert 2 is shown in the as disassembled condition.

Figure 3 – General appearance of the samples insert 1 and 2 in the as received condition.

Macrographic examination of insert 2 shows an oxidation layer probably resulting of the contact with oil from the engine. It can be observed in Fig. (4) the occurrence of corrosion product deposition in the cooling groove.

Figure 4 – Aspect in the groove region of insert 2 with corrosion product deposition.

Figure (5) shows insert 2 after chemical cleaning for deposit removing. It is observed the occurrence of corrosion pits as well through-thickness and non through-thickness cracks in association to corrosion pits. Such pits are aligned along the middle point of the curvature radius as indicated by the arrow in Fig. (5). The same characteristics could be observed in insert 1 as shown in Fig. (6).

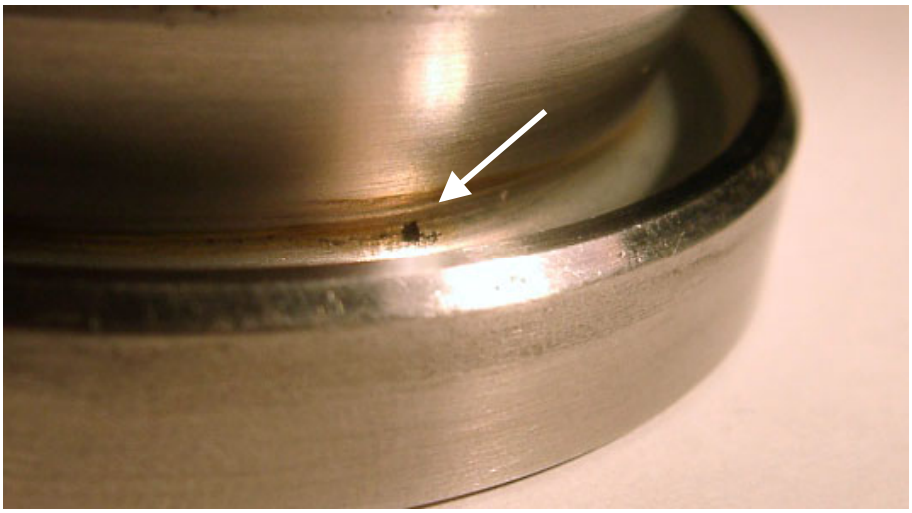

Figure 5 – Corrosion pit observed after cleaning of insert 2 and its associated crack.

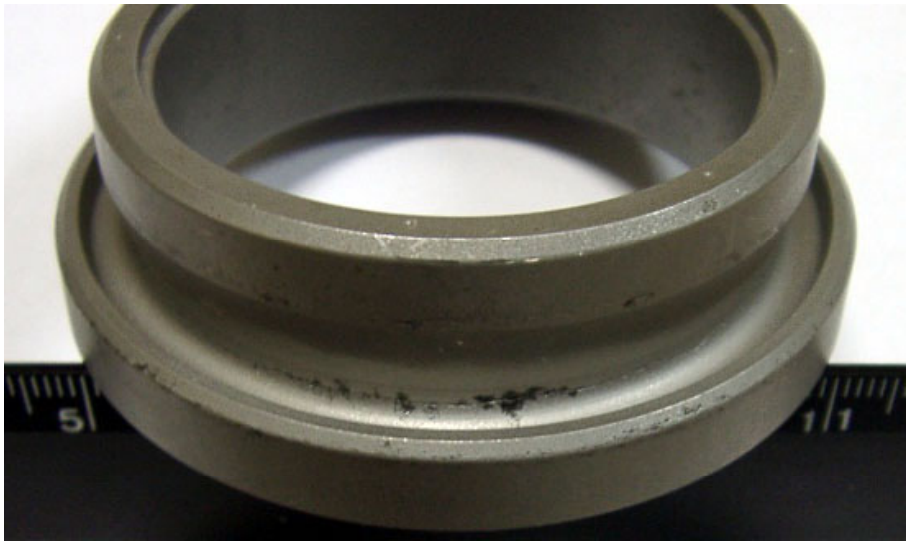

Figure 6 – Corrosion pits associated to cracks observed in insert 1.

2.3. Hardness Test

Rockwell C hardness tests were performed at the face of the inserts. Table (2) shows the results.

Table 2 –Rockwell C Hardness Tests Results.

Sample	1st Imp.	2nd Imp.	3rd Imp.	4th Imp.	5th Imp.	Average
Insert 1	39.7	40.6	41.1	40.4	41.1	40.6
Insert 2	40.8	41.0	39.4	39.7	41.2	40.4

From the hardness tests it can be seen that the values are in accordance to that expected in relation to a SAE 51410 stainless steel in the quenched and tempered condition in the range of 38 HRc to 42 HRc. According to the literature (ASM, 1975), such condition can guarantee maximum resistance to the stress corrosion phenomena and also high mechanical resistance.

2.4. Fracture Surface Analysis – Macroscopic Examination

Despite the high grade of oxidation and some deformation the macrographic analysis of the surface fracture indicates the occurrence of a brittle fracture process. Figure (7) shows the aspect of the surface fracture obtained after a normal cutting to the plane of crack in through-thickness crack section.

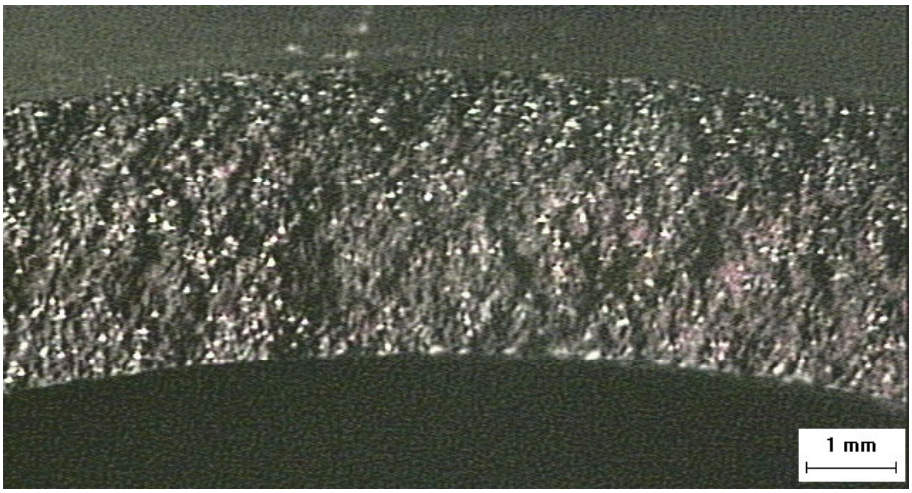

Figure 7 – Surface fracture aspect on insert 1 observed by Stereoscopic Magnifying Glass.

2.5. Metallographic Examination

Optical microscopy analysis was performed for characterization of the failure and material. Figure (8), shows a transversal sample section of insert 1 without chemical etching. It can be observed that the crack begins in the external side of the insert, in the curvature radius, and propagates toward interior in a "zigzag" pattern. In the same section (Fig. 8), other small internal cracks can be observed, which growth would result in the intersection with the larger crack initiated at the external side in a corrosion pit and finally causing the rupture of the section. Figures (9) and (10) show the same cracks of Figs. (7) and (8) with chemical etching. It is possible to note that the crack propagation occurs along the previous austenite grain boundaries, typical aspect of heat treatment crack (quenching-crack) in martensitic stainless steels. Tempered martensite and carbides typical of SAE 51410 stainless steels in the quenched and tempered condition compose the examined microstructure.

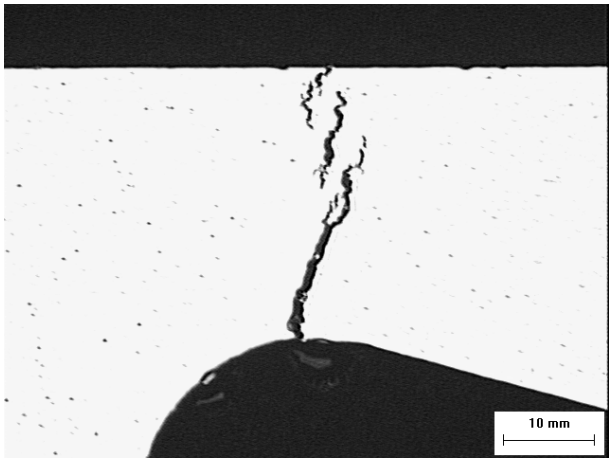

Figure 8 – Morphologic aspect of cracks observed by optical microscopy without etching.

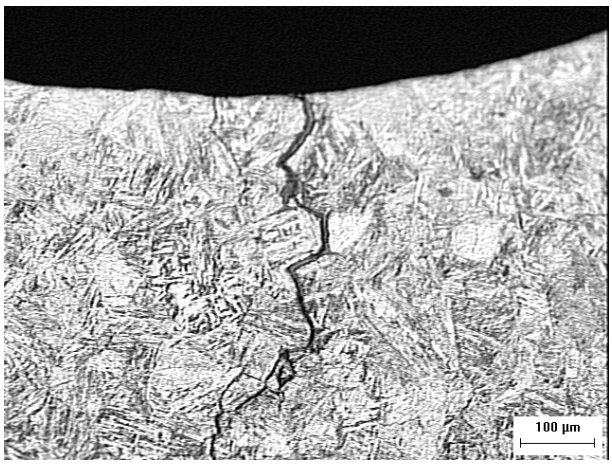

Figure 9 – Detail of crack (internal side) showed at Fig. (8). A preferential path is verified along the previous austenite grain boundaries. Etching: Vilella.

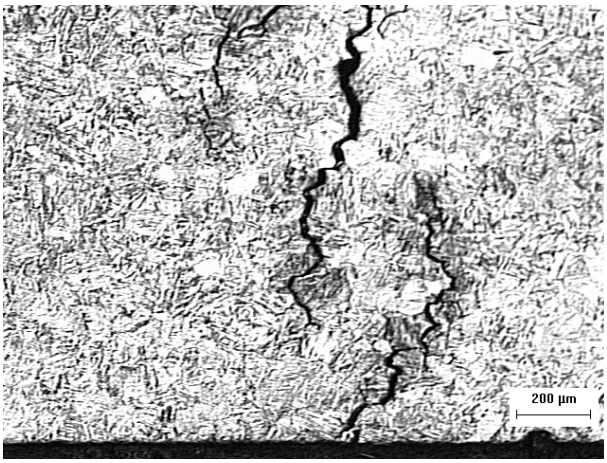

Figure 10 – Detail of internal cracks showed in Fig. (8). Etching: Vilella.

3. Finite Element Model

An axisymmetric finite element thermoelastic model was developed to study the stress distribution present in the insert. The analysis was developed in two stages. In either stage a steady state problem was considered. The mesh obtained after a convergence analysis and the boundary conditions are shown in Fig. (11) for the two stages analyzed. The first one, called *assemblage*, models the assemblage process of the insert in the prechamber engine cylinder head with interference through a process involving subzero cooling, which promotes the development of residual stresses. The interference was modeled supposing a rigid engine head and applying a prescribed radial displacement equal to the interference value on the annular contact surface, between the insert and the engine head. A value of 0.015 mm was considered for the interference in the assemblage stage. The prescribed displacements are represented by the light blue triangles in Fig. (11*a*). The second stage, called *operation*, models the operation condition of the component, which is submitted to a thermomechanical loading. Therefore the combined effects of the temperature rise promoted by the head engine, the heat removal by convection in the cooling groove and the assemblage with interference are analyzed together as a coupled problem. In this stage, the interference value was computed considering the thermal dilation of the engine head and temperature boundary condition were prescribed at the internal (T_{int} = 300°C) and external (T_{ext} = 150°C) insert surfaces. Moreover, convection boundary conditions were prescribed at the cooling groove (h = 1000 W/m^2 K, T_{Fluid} = 80°C) and an initial temperature of 28°C was adopted. The prescribed displacement and the boundary conditions are shown in Fig. (11*b*), with displacements in light blue, temperature in orange and convection in red. In these stage both the temperature and the stresses field developed during operation are estimated. Numerical simulations were performed with commercial finite element code ANSYS (Ansys, 2001). Elements PLANE13 (4 nodes, with 2 degrees of freedom of displacement and 1 degree of freedom of temperature per node) were used. This element considers the coupling between thermal and mechanical phenomena. Its worth to mention that the residual stress

associated with the transient subzero cooling assemblage process, which can promote phase transformation and plastic strain, are not addressed by the numerical simulations presented.

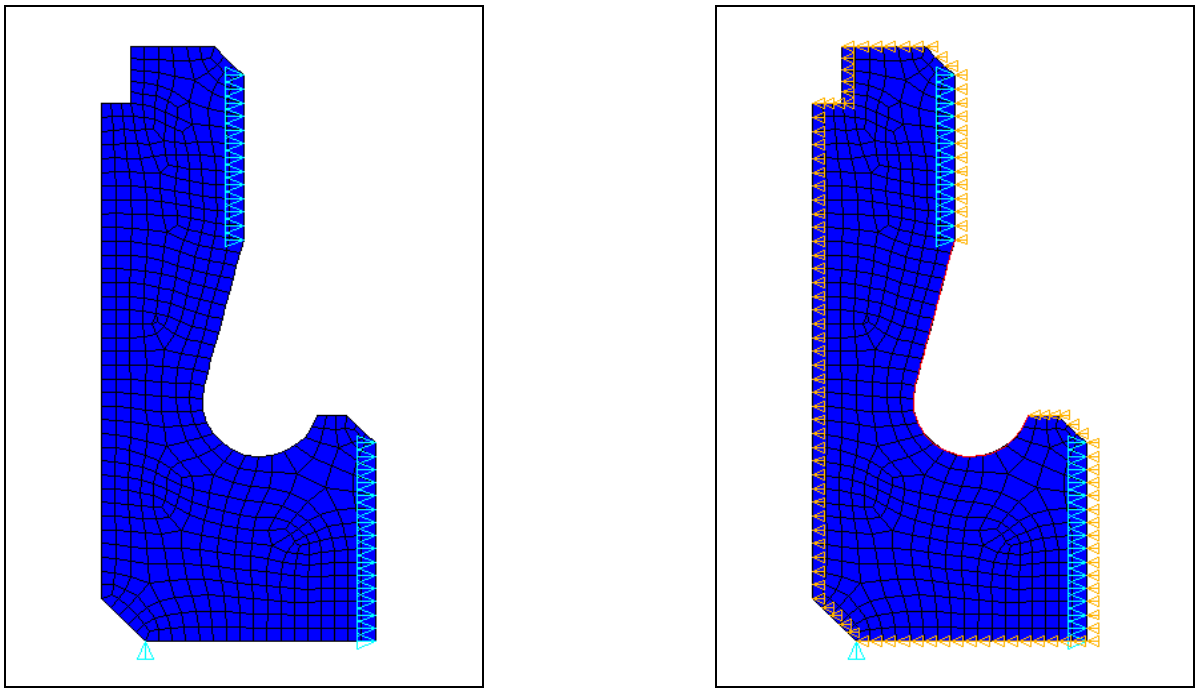

(a) (b)

Figure 11 - Finite element mesh and boundary conditions for the two stages. (a) Assemblage and (b) Operation.

In both stages, it was assumed that the material properties are not temperature dependent and that the material is on the elastic regime. Table (3) lists the thermomechanical properties used in the finite element analysis.

Table 3 –Thermomechanical properties used in the finite element analysis.

	ELEMENT	
Parameter	**Insert**	**Head Engine**
Elastic Modulus (GPa)	220	-
Poisson ratio (-)	0.30	-
Yield Strength (MPa)	1030	-
Tensile Strength (MPa)	1340	-
Density (kg/m^3)	7.7 x 10^3	-
Coefficient of Linear Thermal Dilatation (m/m K)	1.12 x 10^{-5}	1.33 x 10^{-5}
Thermal Conductivity (J/m K s)	25	-
Specific Heat (J/Kg K)	1500	-

4. Numerical Simulations

Numerical simulations were developed to determine the stress and the temperature distributions promoted by the thermomechanical loading in the two stages. Figure (12) presents the results associated with the assemblage stage and Figs. (13) and 14 presents the results associated with the operation stage. For the assemblage stage, the results show a residual tensile stress field normal to the crack plane in the region were the crack developed (Fig. 12*a* and 12*c*). A maximum value of about 220 MPa was observed in the region marked with MX in Figs. (12*a*) and (12*c*). This is the region where cracks develop.

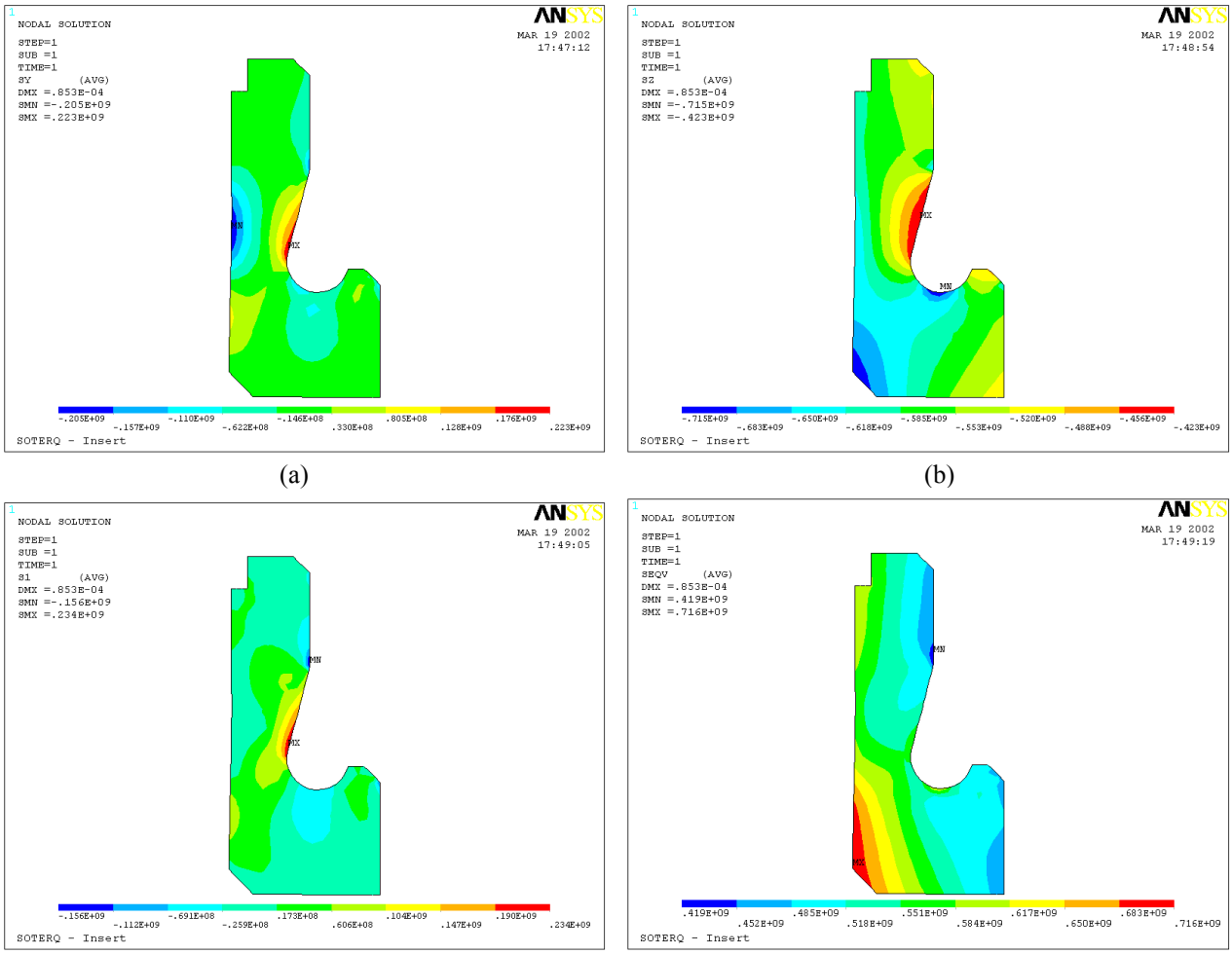

Figure 12 - Finite element analysis. Stress distribution for the assemblage stage. Longitudinal (a), tangential (b), maximum principal (c) and von Mises (d) stress distributions.

For the operation stage, the stress levels increase to about 540 MPa at this same region (MX in Figs. 13*a* and 13*c*). It can be observed from the numerical results that this region is the most likely for the crack propagation. Figures (12*d*) and (13*d*) show the von Mises equivalent stress distribution. Maximum values of 716 MPa and 1150 MPa were observed for the assemblage and operation stages, respectively. The results indicate the absence of plastic deformations during the assemblage stage and a small plastic region during the operation stage (red region in Fig. 13*d*). In spite of the use of an elastic model, it is possible to assume that the presence of plastic deformations in the operation stage do not promote a considerable stress redistribution and, therefore, the elastic model represents a good estimate of the component stress distribution. Figure (14) presents the temperature distribution in the insert. Severe temperature gradients of about 100° C occur through the insert wall, which has a thickness smaller than 5 mm.

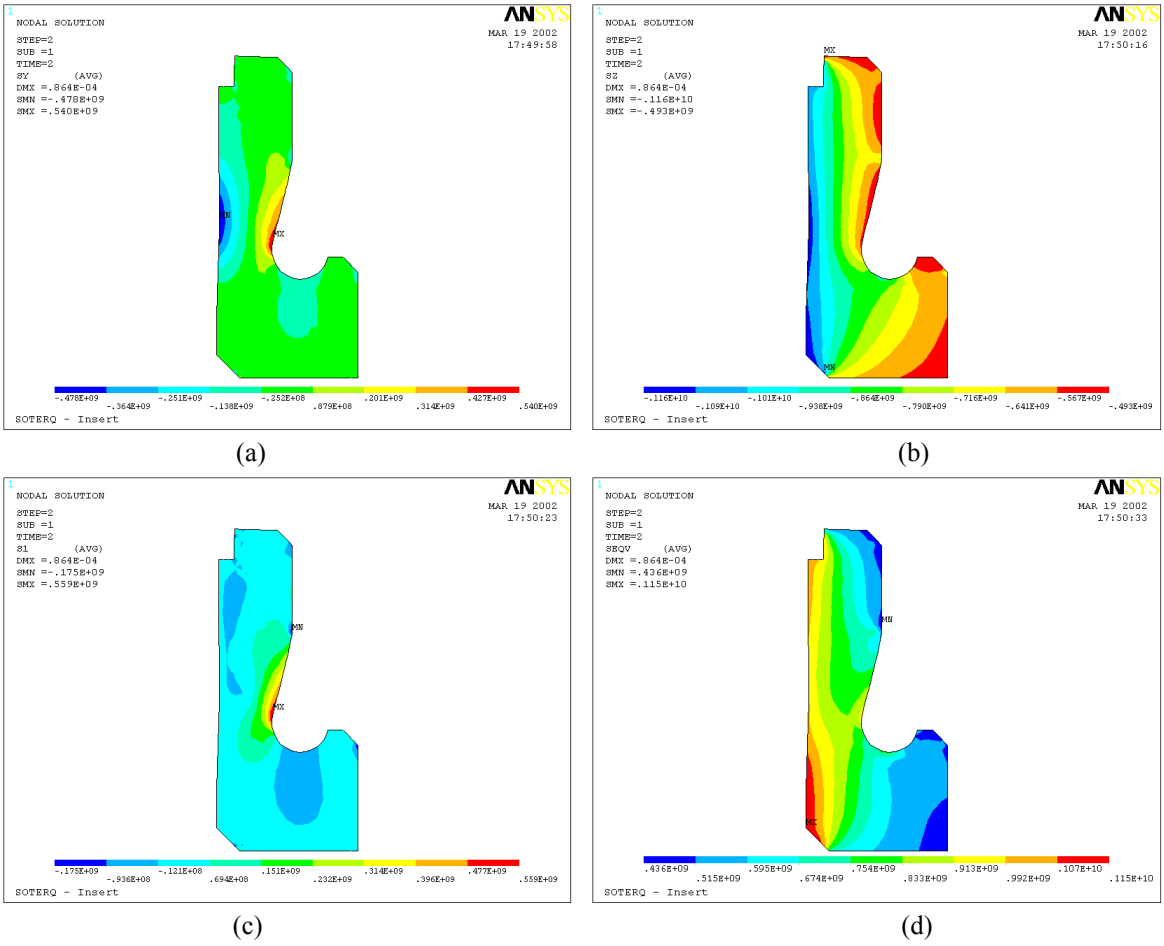

Figure 13 - Finite element analysis. Stress distribution for the operation stage. Longitudinal (a), circumferential (b), principal (c) and von Mises (d) stress distributions.

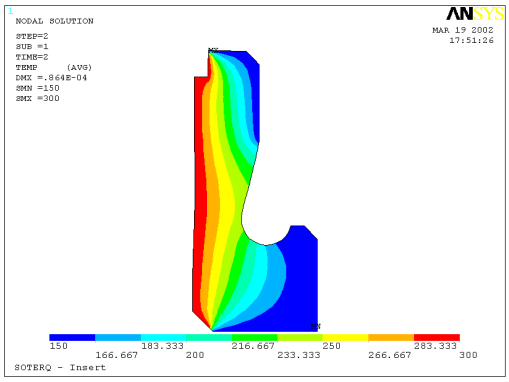

Figure 14 - Finite element analysis. Temperature distribution for the operation stage.

5. Material Considerations and Discussion

It was verified from material analysis the occurrence of corrosion pits associated to cracks, which propagates from internal to external side of the insert. These cracks observed by optical microscopy are characteristic of quenching-cracks by its morphology and localization, that is, intergranular cracks along the previous austenite grain boundaries and particularly the presence of internal cracks to the structure of the component (Figs. 8 and 10), characterizing a stress relieving mechanism due to a thermal shock. It can be observed that the high hardenability and the low thermal conductivity of this type of steel makes it particularly susceptible to the quenching-crack phenomena, being also susceptible to it when submitted to high temperatures gradients or quickly heated. Optical microscopy analysis does not reveal microstructural modifications. It shows a uniform microstructure which is composed by tempered martensite and carbides, typical of a SAE 51410 (martensitic stainless steel) in the quenching and tempered condition. It can be assumed that the stress levels at the region of failure in association to high service temperatures and the medium (cooling fluid) have favored the pit formation. It is worthy of note that the pit attack could also be favored by the formation of corrosion deposits as shown in Fig. (2).

The material and stress analysis results indicate that the interference assemblage technique has contributed for the failure of the insert, as this type of assemblage requires the cooling of the insert to sub-zero temperatures. It is known that the heat treatment of martensitic stainless steels demands care not only on heating but also on cooling. Quenching for hardening can be performed in oil or air being more frequently used oil to avoid warping and cracking, particularly for complex geometry components and/or thickness variations. Martensitic stainless steels have its Ms 90 line (90% of martensite formation) at 280°C. The higher carbon steels such as SAE 51440 C and the higher nickel SAE 51431 are likely to retain large amounts of untransformed austenite is the as-quenched structure, frequently as much as 30% by volume. Despite having less carbon, SAE 51410 Steel can also retain a significant amount of untransformed austenite (Unterweiser et al 1982). The cooling to sub-zero temperature (stabilizing) results in transformation of retained austenite in martensite which is liable to crack unless tempered immediately. For martensitic stainless steels a stabilization heat treatment consists on cooling the component in the range of –75°C to –195°C to transform all retained austenite into martensite. Temper must follow immediately to avoid cracking.

6. Conclusions

A failure analysis of an internal combustion martensitic stainless steel gas engine insert that failed after 6000 hours of operation was developed through a methodology comprising materials and stress analysis standpoint. The study started with a material characterization, involving chemical, hardness and metallographic analysis followed by surface fracture analyses that shown the presence of cracks in critical regions. Finally, numeric simulations with a thermoelastic finite element model were used to estimate the residual stress distributions present in the mechanical component after the assembly process and the stress distribution during operation. From the proposed methodology the following assumptions can be drawn for the failure:

- A heat treatment failure occurred during manufacturing of the insert, which presents retained austenite before the assemblage process. The subzero cooling assemblage process promotes quenching-cracks formation (due to the transformation of the retained austenite in martensite), which tends to growth by the action of tensile stresses in the region indicated as MX in Figs. (12*a*) and (12*c*). Also, a localized heterogeneity in chemical composition due to same heat treatment failure can produce the interruption of the passivation layer favoring the formation of pit corrosion.
- The rupture of the insert has occurred by propagation of quenching-cracks nucleated externally, associated to pits corrosion.
- It was observed that the planes of the cracks propagation are normal to the maximum tensile stress direction as determined by finite element analysis.
- Tensile stresses and residual stresses in association to pit corrosion, quenching cracks and a non-stabilized microstructure has contributed to the failure of component.

Its worth to mention that despite the residual stresses associated with the transient subzero cooling assemblage process, which can promote phase transformation and plastic strain, are not addressed by the numerical simulations presented, the indications obtained by the model, in relation to the action of the tensile stress and temperature operation associated to material characteristics, gives support to the conclusion about the failure.

7. Acknowledgements

The authors would like to acknowledge the support of the Brazilian Research Agency CNPq.

8. References

ASM, 1975, (American Society for Metals), Metals Handbook, Vol.10 *Failure Analysis and Prevention*, Metals Park.

Almer, J.D., Cohen, J.B. and Moran, B., 2000, "The Effects of Residual Macrostresses and Microstresses on fatigue Crack Initiation", *Materials Science and Engineering*, A284**,** pp. 268–279.

Ansys, 2001, "*Reference Manual*" ver.5.7.

Boley, B.A. and Weiner, J.H., 1985, *"Theory of Thermal Stresses"*, Kreiger.

Fuchs, H.O. and Sephens, R.I, 1980, *"Metal Fatigue in Engineering"*, John Wiley & Sons.

Pacheco, P.M.C.L., Savi, M.A. and Camarão, A.F., 2001; "Analysis of Residual Stresses Generated by Progressive Induction Hardening of Steel Cylinders", *Journal of Strain Analysis for Engineering Design*, ISSN 0309-3247, Vol. 36, No.5, pp.507-516.

Pacheco, P.M.C.L., Kenedi, P.P. and Jorge, J.C.F., 2002; "Elastoplastic Analysis of the Residual Stress in Chain Links", *OMAE'2002 - 21st International Conference on Offshore Mechanics and Arctic Engineering*, Olslo, Norway.

SAE, 1988, *"Fatigue Design Handbook"*, SAE – Society of Automotive Engineers.

Unterweiser, P.M., Boyer, H.E. and Kubbs, J.J., 1982, *"Heat Treater's Guide – Standard Practices and Procedures for Steel"*, American Society for Metals, Metals Park, Ohio 44073, pp. 421-426.

Webster, G.A. and Ezeilo, A.N., 2001, "Residual Stress Distributions and their Influence on Fatigue Lifetimes", *International Journal of Fatigue*, 23**,** pp. S375–S383.

9. Copyright Notice